

COSMIC SHEAR: THE DARK SIDE OF THE UNIVERSE

L. VAN WAERBEKE^{1,2}, Y. MELLIER^{1,3}, I. TERENO^{1,4}

¹*Institut d'Astrophysique de Paris*

98bis Bd Arago, 75014, Paris, France

²*Canadian Institute for Theoretical Astrophysics*

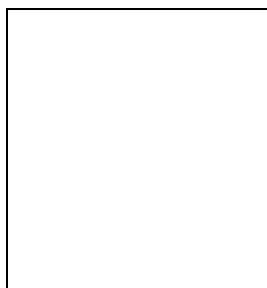
60 St George Str., M5S 3H8, Toronto, Canada

³*Observatoire de Paris, LERMA*

61, avenue de l'observatoire, 75014, Paris, France

⁴*Department of Physics, University of Lisbon*

Campo Grande, Edificio C8, 1749-016 Lisboa, Portugal



We discuss the present status and future prospects for cosmic shear observations and their cosmological constraints. We review the evidences supporting the cosmological origin of the measured signal, and discuss the possible problems coming from intrinsic alignment and the actual limitations of theoretical predictions.

1 Introduction and History

The cosmic shear is a gravitational lensing effect which occurs everywhere in the universe, and allows astronomers to map the projected mass distribution on the sky from the solely observation of the distorted distant galaxies. The idea of mapping the matter using the gravitational deflection of ray-lights was born in 1937 when F. Zwicky^{43,44} envisioned the possibility to use the distorted shape of distant galaxies to probe the matter content in nearby clusters of galaxies. His idea was only discussed seriously 30 years after, when first detailed analytical work were produced^{24,11}, motivated by the progress made in geometric optic in curved spacetimes³³. But it is only in the early 90's that a robust link was established between an appealing theoretical idea and the observational possibilities^{27,6,21}. In the meantime, in 1983, a first attempt to measure cosmic shear failed³⁷ mainly because of the poor image quality of data available at that time. The interest for cosmic shear raised again after the discovery of giant arcs in 1987, and the burst of theoretical papers started in the mid 90's^{41,4,19}, followed by many others³. In 2000 the first detections were reported almost simultaneously, and independently by four teams^{1,23,38,42}. Since

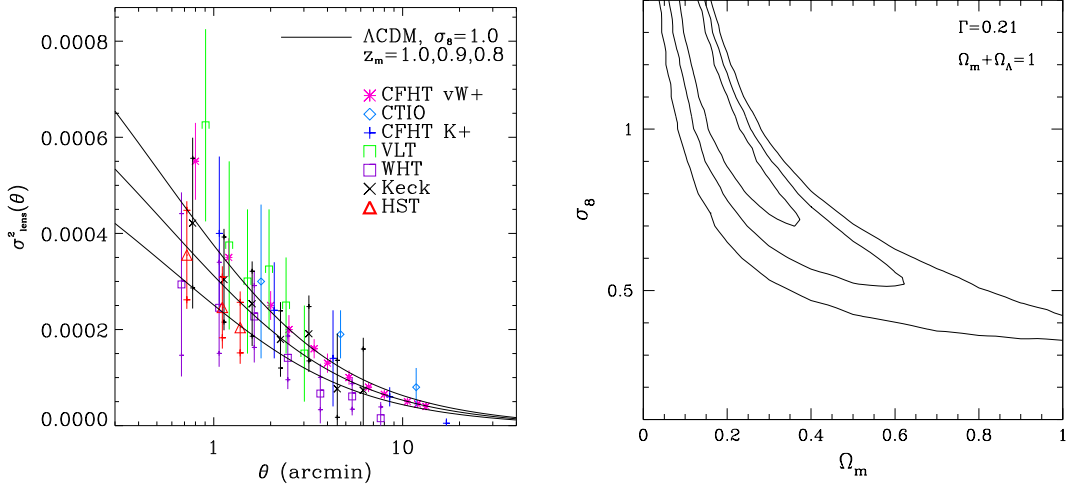


Figure 1: Left: compilation of recent results of top-hat shear variance measurements from several groups³¹. Right: Ω_m , σ_8 constraints for the Red Sequence Cluster Survey (RCS) from the shear top-hat variance measurements¹⁷.

then, several other measurements were done and significant improvements in the data analysis lead to refined measures and to the first robust cosmological constraints^{26,40,32,30,39,17,12,16,2,31}.

2 Theory

Gravitational lensing plays a special role in cosmology because it is the only way to see the dark matter distribution from the galactic scale up to several degrees. It is therefore the only observational tool which can measure directly the mass power spectrum in the nearby universe with a direct link to the constituents of the universe simultaneously in the linear and non-linear dynamical regimes.

The power spectrum of the projected mass, called the convergence power spectrum $P_\kappa(k)$, is the quantity which relates any cosmic shear two points statistics to the cosmological parameters and the 3-dimensional mass power spectrum $P_{3D}(k)$:

$$P_\kappa(k) = \frac{9}{4}\Omega_0^2 \int_0^{w_H} \frac{dw}{a^2(w)} P_{3D} \left(\frac{k}{f_K(w)}; w \right) \left[\int_w^{w_H} dw' n(w') \frac{f_K(w' - w)}{f_K(w')} \right]^2, \quad (1)$$

where $f_K(w)$ is the comoving angular diameter distance out to a distance w (w_H is the horizon distance), and $n(w(z))$ is the redshift distribution of the sources. The mass power spectrum $P_{3D}(k)$ is evaluated in the non-linear regime²⁸, and k is the 2-dimensional wave vector perpendicular to the line-of-sight. The three most common observables are respectively the shear top-hat variance^{27,6,21}, the aperture mass variance^{22,34} and the shear correlation function^{27,6,21}:

$$\langle \gamma^2 \rangle = \frac{2}{\pi\theta_c^2} \int_0^\infty \frac{dk}{k} P_\kappa(k) [J_1(k\theta_c)]^2, \quad (2)$$

$$\langle M_{\text{ap}}^2 \rangle = \frac{288}{\pi\theta_c^4} \int_0^\infty \frac{dk}{k^3} P_\kappa(k) [J_4(k\theta_c)]^2, \quad (3)$$

$$\langle \gamma(r)\gamma(r+\theta) \rangle_r = \frac{1}{2\pi} \int_0^\infty dk k P_\kappa(k) J_0(k\theta), \quad (4)$$

where J_n is the Bessel function of the first kind. They are all different measurements of the same physical quantity, the convergence power spectrum $P_\kappa(k)$. Their internal consistency provides a valuable check of the cosmological origin of the observed signal.

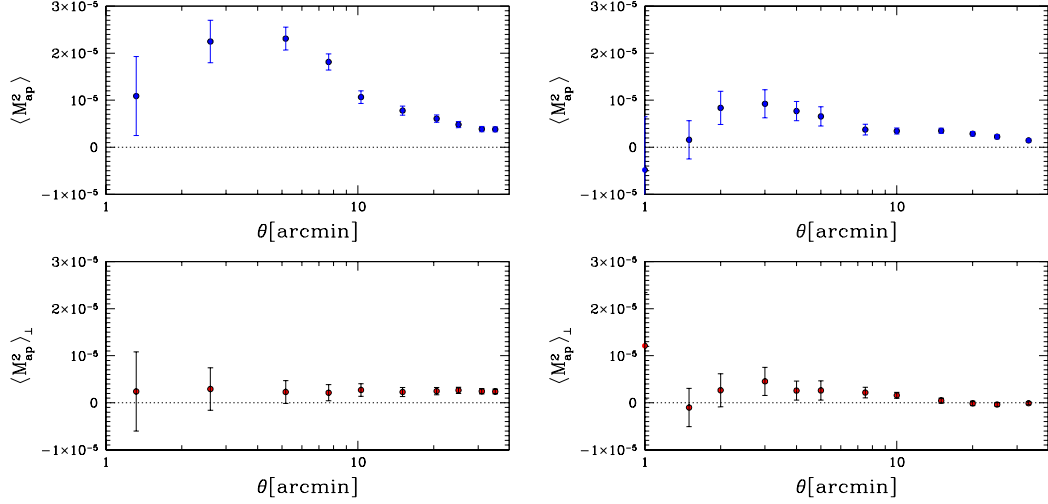


Figure 2: Left: E (top) and B (bottom) modes measured in the VIRMOS survey³⁹. Right: E (top) and B (bottom) modes measured in the RCS survey¹⁶. The B mode is low and the E mode compatible with the predictions for the aperture mass statistics³⁴.

3 Measurements and cosmological constraints

As quoted earlier¹⁹, the cosmic shear signal depends primarily on four parameters: the cosmological mean density Ω_m , the mass power spectrum normalisation σ_8 , the shape of the power spectrum Γ , and the redshift of the sources z_s . Therefore any measurement of the statistics shown in Section 2 could provide constraints on these parameters. Left plot on Figure 1 shows a compilation of the measurements of the top-hat variance done by different groups, compared with a typical Λ CDM model. The agreement of these measurements, done by different people, and with different telescopes, support the idea of cosmological origin of the signal. The right plot on Figure 1 shows the constraints on Ω_m and σ_8 obtained from the top-hat variance of the shear measured in the Red Sequence Cluster survey¹⁷. Strong assumption have been applied to the hidden parameters Γ and the source redshift, which allows to break the degeneracy between Ω_m and σ_8 (see also⁴⁰). However, the top-hat variance is a rather weak statistics, in the sense it does not provide direct checks of possible contamination by systematic effects (like residual optical distortion and telescope tracking, or intrinsic alignment). For this reason, various tests have been proposed and developed to provide robust checks of the lensing effects, and to quantify the cosmological origin of the signal. They are the following:

- The E , B modes decomposition separates the lensing signal into curl and curl-free modes¹⁰. It is expected, and it can also be quantified on the star field, that residual systematics equally contributes to E and B , while the lensing signal should be present ONLY in the E mode because gravity derives from a true scalar field³⁶. The E mode is identical to the aperture mass statistics Eq.(3)^{22,34}. The E and B modes have been measured in several surveys^{40,39,30,16}, and support the cosmological origin of the signal, as well as showing the already small amount of residual systematics achieved with today's technology. Figure 2 shows such measurements for the VIRMOS^{a,b} and RCS^c surveys.

- The self-consistency of the three statistics shown in Section 2 was shown for the VIRMOS^{40,30} and RCS surveys^{17,16}.

- The lensing signal is expected to decrease for low redshift sources, just because the gravita-

^a<http://www.astrsp-mrs.fr>

^b<http://terapix.iap.fr/DESCART>

^c<http://www.astro.utoronto.ca/gladders/RCS/>

Name	σ_8	statistic	field	CosVar	E/B	Prior z_s	Prior Γ
Maoli et al. 01	1.03 +/-0.05	$\langle \gamma^2 \rangle$	VLT+CTIO+ WHT+CFHT	no	no	-	0.21
Rhodes et al. 01	0.91 +0.25-0.29	$\langle \gamma(\mathbf{r})\gamma(\mathbf{r}+\theta) \rangle_z$	HST 0.05 sq.deg.	yes	no	0.9-1.1	0.25
LVW et al. 01	0.88 +/-0.11	$\langle \gamma^2 \rangle$ $\langle M_{ap}^2 \rangle$ $\langle \gamma(\mathbf{r})\gamma(\mathbf{r}+\theta) \rangle_x$	CFHT 8 sq.deg.	no	no	1.1	0.21
Hoekstra et al. 01	0.81 +/-0.08	$\langle \gamma^2 \rangle$	CFHT+CTIO 24 sq.deg.	yes	no	0.55	0.21
Bacon et al. 02	0.97 +/-0.13	$\langle \gamma(\mathbf{r})\gamma(\mathbf{r}+\theta) \rangle_z$	Keck+WHT 1.6 sq.deg.	yes	no	0.7-0.9	0.21
Refregier et al. 02	0.94 +/-0.17	$\langle \gamma^2 \rangle$	HST 0.36 sq.deg.	yes	no	0.8-1.0	0.21
LVW et al. 02	0.94 +/-0.12	$\langle M_{ap}^2 \rangle$	CFHT 12.5 sq.deg.	yes	yes	0.78-1.08	0.1-0.4
Hoekstra et al. 02	0.91 +0.05-0.12	$\langle M_{ap}^2 \rangle$	CFHT+CTIO 53 sq.deg.	yes	yes	0.54-0.66	0.05-0.5

Figure 3: Constraints on σ_8 for a flat cosmology with $\Omega_m = 0.3$. The meaning of the different columns are: statistics; which statistic is used (see Section 2), field; telescope used and area observed, CosVar; whether or not cosmic variance has been included in the error bars, E/B; whether or not the E , B mode separation has been used, Prior z_s ; flat prior on the mean source redshift applied, Prior Γ ; flat prior on Γ applied.

tional distortion becomes less efficient. This decrease of the signal has been observed recently for the first time, when comparing the VIRMOS survey aperture mass³⁹ which has a source mean redshift around 0.9 to the RCS which has a source mean redshift around 0.6. The expected decrease in signal amplitude is about 2, which is what is observed (see Figure 2).

-Space images provide in principle systematics-free environment, and even if the observed areas are still smaller than ground based observations, space data provide ideal calibrations of the cosmic shear signal^{32,12,31}, which are in excellent agreement with ground based measurements.

Figure 3 shows the constraints on σ_8 obtained for a flat cosmology with $\Omega_m = 0.3$ for various surveys, statistics and priors. There is an overall good agreement, and some preference is given for a normalisation slightly smaller than 1 (a comparison with cluster normalisation results is given elsewhere³⁹).

4 Comments

Gravitational lensing is not the only natural process which produces alignment of galaxies over large distances. Intrinsic alignment might occur from tidal fields, and produce galaxy shape correlations over cosmological distances, and contaminate cosmological signal^{7,8,14,29,9,13}, which should in principle split, in a predictable way, into E and B modes. There is unfortunately only partial agreement between these different approaches. Yet it is hard to have a robust prediction for the intrinsic alignment effect, although it is not believed to be higher than a 10% contribution for a lensing survey with a mean source redshift at $z_s = 1$. A recent work²⁰ suggested that intrinsic alignment could dominate the cosmic shear even in deep surveys, which seems incompatible with the observations: this would indeed imply a very low $\sigma_8 \sim 0.1$ and we

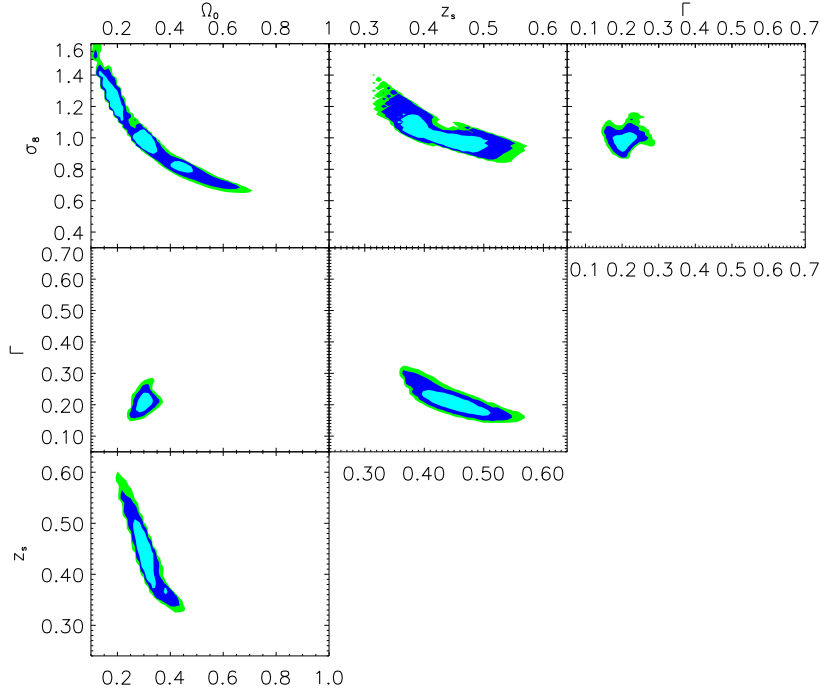


Figure 4: 1, 2 and 3σ contours for the parameters Ω_m , σ_8 , Γ and z_s , assuming a 130 sq.deg. survey and $m_{IAB} = 24.5$. Constraints are obtained from the measurement of the shear correlation function from $0.6'$ to $30'$. On each plot, hidden parameters are marginalised as defined in the text. The true model is $\Omega_m = 0.3$, $\sigma_8 = 1.$, $\Gamma = 0.21$ and $z_s = 0.44$. Note that, because of the chosen parametrisation, the mean redshift of the survey is $2z_s$.

should also observe an increase of the effect as we go from deep to shallow survey, which is not the case (see Figure 2). In any case, intrinsic alignment contamination can be removed completely by measuring the signal correlation between distant redshift bins, instead of measuring the full projected signal.

Another issue is the cosmological parameter determination, which relies on the accuracy of the non-linear prediction of the cosmic shear signal. The non-linear predictions²⁸ are only accurate to $\sim 10\%$ ³⁹, which limitates the measurement of cosmological parameters to the same accuracy. Therefore a net progress on non-linear predictions will have to be made before cosmic shear measurements can provide high-precision constraints on the parameters.

5 The Future

Over the next 5 years, the Canada France Hawaii Telescope Legacy Survey (CFHTLS) will produce 130 sq.deg. of high image quality data down to $m_{IAB} = 24.5$. The observations in 5 colors will allow a good determination of photometric redshifts, and the large area will provide accurate measurements of the projected mass power spectrum from $l = 90$ to $l = 10^5$. Provided that residual systematics can be eliminated, accurate cosmological parameter determination will be possible, and the joint analysis with other experiments (CMB, 2dF, SLOAN) will break parameter degeneracies (Van Waerbeke et al. in preparation). Figure 4 is an example of constraints on Ω_m , σ_8 , Γ and z_s , where the hidden parameters of each plot have been marginalised using the priors $\Omega_m \in [0.25, 0.35]$, $\sigma_8 \in [0.95, 1.05]$, $\Gamma \in [0.1, 0.3]$, $z_s \in [0.4, 0.5]$. The true model is $\Omega_m = 0.3$, $\sigma_8 = 1.$, $\Gamma = 0.21$ and $z_s = 0.44$ (the mean source redshift is $2z_s$). Error bars contain gaussian cosmic variance³⁵ and statistical noise corresponding to $m_{IAB} = 24.5$ ³⁹. It is clear that accurate constraints can be obtained, but it is also very important to estimate the redshift distribution, as Figure 4 shows that the redshift axis is always strongly degenerate.

New roads have also been recently opened. The shear three point function has probably

been detected⁵, which potentially is a direct measure of Ω_m ⁴. The very first measurement of the bias from cosmic shear has also been claimed^{15,18} which paved the way for galaxy formation studies from cosmic shear.

References

1. D.J. Bacon, A.R. Réfrégier, R.S. Ellis, MNRAS **318**, 625 (2000)
2. D. Bacon, R. Massey, A. Réfrégier, R. Ellis, astro-ph/0203134
3. M. Bartelmann, P. Schneider, *Phys. Rep.* **340**, 291 (2001)
4. F. Bernardeau, L. Van Waerbeke, Y. Mellier, A& A **322**, 1 (1997)
5. F. Bernardeau, Y. Mellier, L. Van Waerbeke, A& A in press, astro-ph/0201032
6. R. Blandford, A. Saust, T. Brainerd, J. Villumsen, MNRAS **251**, 600 (1991)
7. R.A.C. Croft, & C.A. Metzler, ApJ **545**, 561 (2001)
8. P. Catelan, M. Kamionkowski, & R.D. Blandford, MNRAS **320**, L7 (2001)
9. P. Catelan, C. Porciani, MNRAS **323**, 713 (2001)
10. R. Crittenden, P. Natarayan, Ue-Li Pen, T. Theuns, ApJ **568**, 20 (2002)
11. J.E. Gunn, ApJ **150**, 737 (1967).
12. H. Haemmerle, J.-M. Miralles, P. Schneider et al., A& A **385**, 743 (2002)
13. S. Hatton, S. Ninin, MNRAS **322**, 576 (2001)
14. A.F. Heavens, A. Refregier, & C.E.C. Heymans, MNRAS **319**, 649 (2000)
15. H. Hoekstra, H. Yee, M. Gladders, ApJ **558**, L11 (2001)
16. H. Hoekstra, H. Yee, M. Gladders, ApJ, in press, astro-ph/0204295
17. H. Hoekstra, H. Yee, M. Gladders et al., ApJ, in press, astro-ph/0202285
18. H. Hoekstra, L. Van Waerbeke, M. Gladders et al., ApJ in press, astro-ph/0206103
19. B. Jain, U. Seljak, ApJ **484**, 560 (1997)
20. Y.P. Jing, submitted to MNRAS, astro-ph/0206098
21. N. Kaiser, ApJ **388**, 272 (1992)
22. N. Kaiser et al., 1994, in Durret et al., *Clusters of Galaxies*, Eds Frontières.
23. N. Kaiser, G. Wilson, G. Luppino, astro-ph/0003338
24. J. Kristian, R.K. Sachs, ApJ **143**, 379 (1966).
25. J. Mackey, M. White, & M. Kamionkowski, MNRAS **332**, 788 (2002)
26. R. Maoli, L. Van Waerbeke, Y. Mellier, et al., A& A **368**, 766 (2001)
27. J. Miralda-Escudé, ApJ **380**, 1 (1991)
28. J. Peacock & S. Dodds, MNRAS **280**, 19 (1996)
29. Ue-Li Pen, L. Jounghun, & U. Seljak, ApJ **543**, 107 (2000)
30. Ue-Li Pen, L. Van Waerbeke, Y. Mellier, ApJ **567**, 31 (2002)
31. A. Réfrégier, J. Rhodes, E. Groth, ApJL, in press, astro-ph/0203131
32. J. Rhodes, A. Réfrégier, E. Groth, ApJ **552**, 85 (2001)
33. R.K. Sachs, Proc. Roy. Soc. London **A264**, 309 (1961).
34. P. Schneider, L. Van Waerbeke, B. Jain, G. Kruse, ApJ **333**, 767 (1998)
35. P. Schneider, L. Van Waerbeke, M. Kilbinger, Y. Mellier, astro-ph/0206182
36. A. Stebbins, 1996, astro-ph/9609149
37. F. Valdes, J. Jarvis, J. Tyson, ApJ **271**, 431 (1983)
38. L. Van Waerbeke, Y. Mellier, T. Erben, et al., A& A **358**, 30 (2000)
39. L. Van Waerbeke, Y. Mellier, R. Pello et al., A& A, in press, astro-ph/0202503
40. L. Van Waerbeke, Y. Mellier, M. Radovich, et al., A& A **374**, 757 (2001)
41. J. Villumsen, MNRAS **281**, 369 (1996)
42. D.M. Wittman, J.A. Tyson, D. Kirkman, et al. , *Nature* **405**, 143 (2000)
43. F. Zwicky, *Phys. Rev.* **51**, 290 (1937).
44. F. Zwicky, *Phys. Rev.* **51**, 679 (1937).